Nonlinear Computational Edge Detection Metalens

Junxiao Zhou, Junxiang Zhao, Qianyi Wu, Ching-Fu Chen, Ming Lei, Guanghao Chen, Fanglin Tian, and Zhaowei Liu*

Optical image processing and computing systems provide supreme information processing rates by utilizing parallel optical architectures. Existing optical analog processing techniques require multiple devices for projecting images and executing computations. In addition, those devices are typically limited to linear operations due to the time-invariant optical responses of the building materials. In this work, a single metalens with an illumination intensity dependent coherent transfer function (CTF) is proposed and experimentally demonstrated, which performs varying computed imaging without requiring any additional optical components. The metalens consisting of nanoantenna structures with a static geometric phase and a nonlinear metallic quantum well layer offering an intensity-dependent dynamic phase results in a continuously tunable CTF. The approach allows for a weighted summation of two designed functions based on the metalens design, which potentially enables all optical computations of complex functions. The nonlinear metalens may lead to important applications in optical neural networks and parallel analog computing.

1. Introduction

Optical lenses are indispensable elements in imaging systems. Conventional lenses exploit refraction to form images on an imager and preserve abundant information of the object, [1] but commonly require additional numerical postprocessing to extract useful information in many cases. Contrary to digital signal processing, optical analog image processing can rid the cumbersome optical-electrical conversion components and process images at much higher speed with lower power consumption. One of the most fundamental operations in optical analog image processing is the edge detection, which mimics one of the critical stages of human visual perception. It preserves the important periphery geometry of the object and significantly reduces the data volumes to be processed. Traditionally, optical edge detection can be achieved by either optical transfer function modulation at the Fourier plane by angular spectrum filters, such as aperture obscurations^[2] and Laplacian operator based on photonic crystals^[3,4] and nonlocal

J. Zhou, J. Zhao, Q. Wu, C.-F. Chen, M. Lei, G. Chen, F. Tian, Z. Liu Department of Electrical and Computer Engineering University of California San Diego, CA 92093, USA E-mail: zhaowei@ucsd.edu

The ORCID identification number(s) for the author(s) of this article can be found under https://doi.org/10.1002/adfm.202204734.

DOI: 10.1002/adfm.202204734

effect or point spread function modulation in the real space by surface-plasmon resonance,^[5] Brewster effect,^[6,7] Goos–Hänchen shift,^[8] spin Hall effect^[9–11] on traditional prisms or polarizers.

Recently, metasurface composed of nanostructure arrays have been proved to be a competent tool for phase, amplitude, and polarization manipulation of light and further developed for a lot of applications.[12-25] Various metasurface designs have been demonstrated to achieve highly efficient optical spatial differentiation. [26-35] Nonetheless, all these methods mentioned have two notable weaknesses. First, the imaging and the signal processing functions are achieved by different optical components in the system. A single device performing imaging and analog processing simultaneously will greatly miniaturize the whole system and provide a higher degree of integra-

tion capability for portable and wearable platforms. Second, and most importantly, traditional metasurfaces are all made by linear and time-invariant materials and are therefore incapable to incorporate any nonlinear operations. Optical nonlinearities have seen increasing demand in all optical computations. [36,37] An integrated nonlinear analog computing device is highly desirable for nontrivial computing applications.

Here, we propose and experimentally demonstrate a single metalens for nonlinear computational imaging without requiring any additional optical components. The geometric phase of the exemplary metalens forms a pair of overlapping sheared images. By employing metallic quantum wells with intensity-dependent optical constants, the phase difference of the two sheared images could be altered by the input intensity, which results in a controllable coherent transfer function (CTF) tuned by the illumination intensity, producing various computed imaging results between an edge image and a diffracted full image. The nonlinear computational metalens can be also expanded to other complicated analog computing applications including optical neural networks and parallel computations and paves the way for multifunctional and miniaturized device.

2. Results

The proposed nonlinear computational metalens and its functions are schematically illustrated in Figure 1. The metalens consists of a bottom gold reflector, a stack of TiN/Al_2O_3 quantum wells, an Al_2O_3 spacer and a gold nanoantenna layer.

www.advancedsciencenews.com

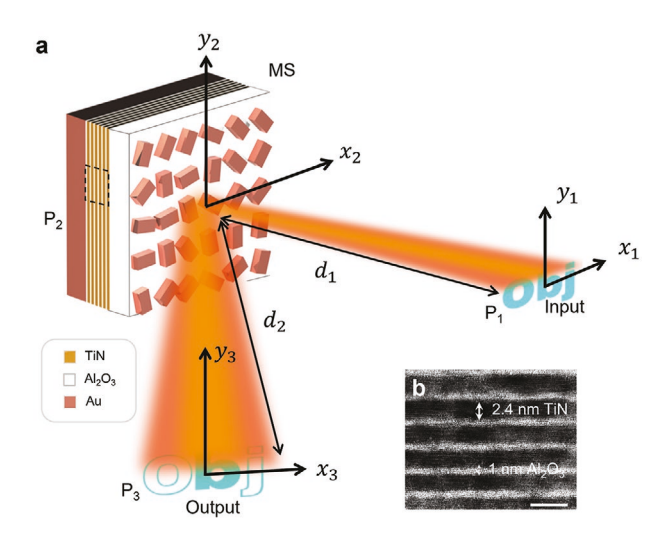


Figure 1. Schematic illustration of the nonlinear computational imaging metalens. a) An edge-detection image is obtained in the high intensity region (indicated as orange color), while diffracted full images are obtained in the low intensity regions (indicated as red color). b) The transmission electron microscopes (TEM) image of the metallic quantum wells with 6 pairs of TiN/Al₂O₃ of black dashed frame in a). Scale bar, 5 nm

The metalens relies on the resonators-on-a-mirror structure to tailor a phase profile and form an image of an object in its reflection mode. Because the TiN quantum wells possess giant Kerr nonlinearity, [38] the optical constants of the TiN/Al₂O₃ multilayers and thus the resultant phase of the metalens becomes tunable with respect to the local illumination intensity. Therefore, this nonlinear metalens acts as not only an imaging element but also an image processing element, which transforms the image by superimposing an additional phase profile defined by the intensity distribution in space. For instance, a diffracted full image of the object is obtained where the intensity is high, while edge images are formed where the intensity is low (see Figure 1).

As shown in Figure 1a, we denote the input electrical field of the object at Plane P_1 as $E_1(x_1, y_1)$. Applying the scalar diffraction with Fresnel approximation, the electrical field E_2 on Plane P_2 , i.e., the location of the metalens, is

$$E_{2}(x_{2}, y_{2}) = s\left(x_{2}, y_{2}; \frac{1}{d_{1}}\right) \mathcal{F}\left[s\left(x_{1}, y_{1}; \frac{1}{d_{1}}\right) E_{1}(x_{1}, y_{1})\right]$$
(1)

where $s\left(x,y;\frac{1}{d}\right) = \exp\left[\frac{i\pi(x^2+y^2)}{\lambda d}\right]$ is a quadratic phase term

and \mathcal{F} is the Fourier-transform operator. Using Dirac bracket notation, the electrical field E_2 right after the reflection from the metalens at plane P_2 is described by

$$|E_{2}^{'}\rangle = T_{MS}(x, y)|E_{2}\rangle = \cos\left(\frac{\phi}{2}\right)|E_{2}\rangle - i\sin\left(\frac{\phi}{2}\right)$$
$$\times \left[\langle R, L|E_{2}\rangle \exp(\mp i2\theta)|L, R\rangle\right]$$
(2)

Here, $T_{\rm MS}(x,y)$ is the Jones Matrix of the metasurface, ϕ is the phase retardation between the long and short axes of a metalens nanoantenna, which is determined by the local resonances and

can be tuned by the incident intensity through Kerr effect. θ is the orientation of the nanoantenna which offers a geometric phase of 2θ . $\langle R, L|E_2\rangle$ is the inner product with right-handed circular polarization (RCP) or left-handed circular polarization (LCP) component (see the Supporting Information Section S1, the theory of MS design, for more information).

Without loss of generality, for the LCP incident light, the tunable phase profile p of the metalens due to the change in local birefringence caused by the intensity controlled optical constant of the nonlinear metallic multilayers could be expressed as

$$p = \exp\left\{i \times \arg\left[\left\langle E_{2}^{'}(0,0) \mid E_{2}^{'}(x,y)\right\rangle\right]\right\}$$
$$= \exp\left(i\theta\right) \exp\left[-i\arctan\left(\cos\phi\tan\theta\right)\right]$$
(3)

To achieve edge detection function as an example, the geometric phase 2θ of the metalens is designed as a summation of two laterally-shifted lens phases with identical focal length f differed by phase π , i.e., $2\theta = \arg[g(x-\Delta,y;f)-g(x+\Delta,y;f)]$, in which $g(x\pm\Delta,y;f)=\exp\{-i\pi[(x\pm\Delta)^2+y^2]/(2\lambda f)\}$ are two converging lens phases with laterally shifted foci located at $(\Delta,0)$ and $(-\Delta,0)$, respectively, as shown in **Figure 2**a,b. The summation of the two lenses leads to intensity subtraction in the overlapped region, leading to a laterally differentiated intensity distribution.

When the incident light intensity is tuned such that the phase retardation φ is π , the input electrical field is completely converted from LCP into RCP. The phase profile $p = \exp(i2\theta)$ is a pure geometric phase distribution. By multiplying Equation (1) and the expression of p, and applying the Fresnel propagator, the electric field in the image plane P_3 is

$$E_{3}(x_{3}, y_{3}) \propto \left\{ \left[\delta(x_{3} - \Delta') - \delta(x_{3} + \Delta') \right] * \left[E_{1}\left(\frac{x_{3}}{M}, \frac{y_{3}}{M}\right) s\left(x_{3}, y_{3}; \frac{d_{1}}{d_{2}^{2}}\right) \right] \right\}$$

$$(4)$$

where $M=-\frac{d_2}{d_1}$ is the magnification and $\Delta'=\frac{d_2}{f}\Delta$ is the shear amount which determines the edge resolution. To simplify the equation, we set $d_1=d_2$. The symbol * represents the convo-

lution operation. When
$$\Delta \ll f$$
, $E_3(x_3, y_3) \simeq 2\Delta' \frac{\mathrm{d}E_1\left(\frac{x_3}{M}, \frac{y_3}{M}\right)}{\mathrm{d}x_3}$

Similarly, if a phase profile of two pairs of lenses with both horizontally and vertically shifted foci is implemented, i.e., $2\theta = \arg[g(x+\Delta,\gamma+\Delta;f) - (x-\Delta,\gamma+\Delta;f) + g(x-\Delta,\gamma-\Delta;f) - g(x+\Delta,\gamma-\Delta;f)]$, we can realize the 2D edge detection along both x and y directions, as will be shown in the next section of this work. More theoretical derivation can be found in the theory derivation of spatial differentiation, Section S2 of Supporting Information.

For phase retardation ϕ between 0 and π , the phase profile of the metalens contains additional dynamic component other than purely the geometric phase, which obstructs the spatial differentiation approximation. The response of the imaging system will be the intensity-controlled weighted superposition of the diffracted full image and the edge image. When the phase retardation is tuned by the incident intensity such that $\phi=0$, the output of the metalens, according to Equation (2), is equal to E_2 . In this case, the metalens is effectively a mirror.

www.afm-journal.de

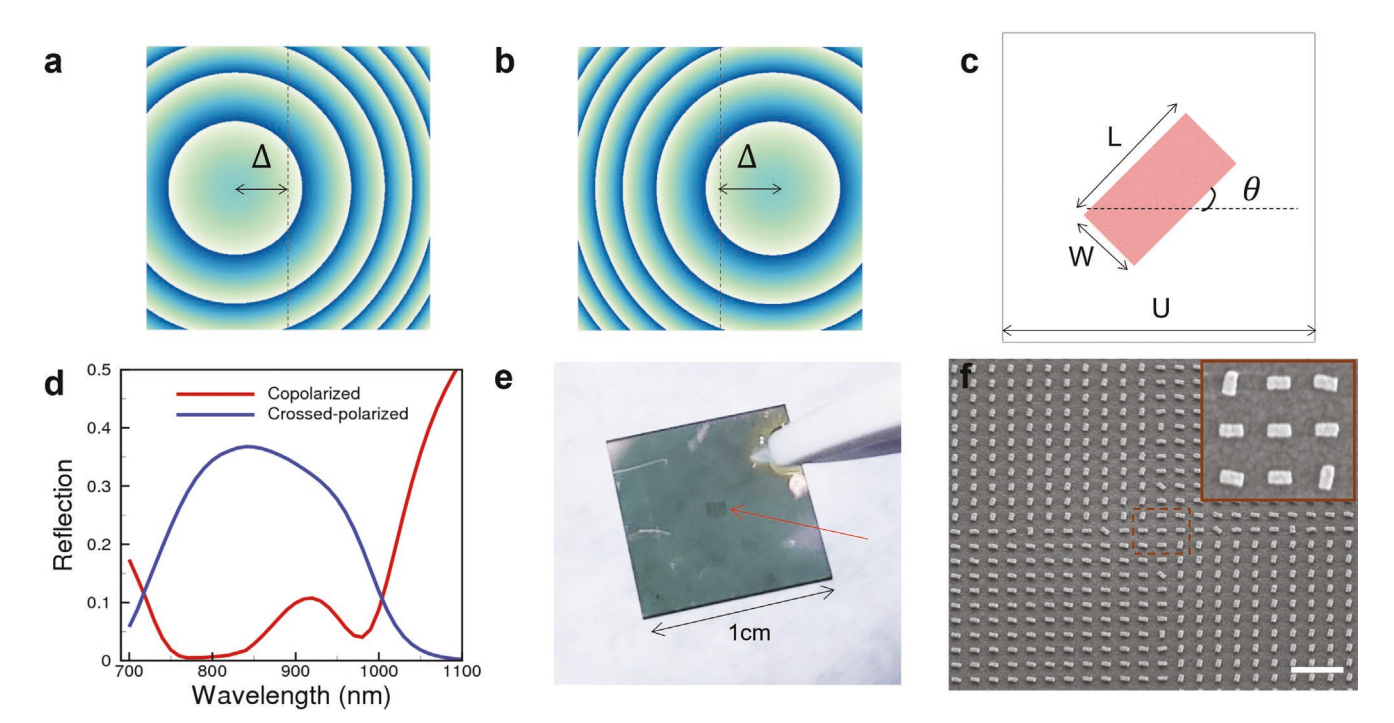


Figure 2. Nonlinear edge imaging metalens design and fabrication. a,b) Two spherical wavefronts with optical axis offset of 2Δ . c) One unit cell of the nanoantena designed of the metalens. θ indates the orientation of the nanobar. d) Wavelength dependent reflection of copolarized light and crossed polarizated light of the metalens. e) The photo of the metalens sample. f) Perspective view SEM image of the metalens. Scale bar, 1 μm. Inset, top view of the enclosed region.

In other words, the function of the metalens can be tuned by the intensity of the light from a mirror to an edge detection imaging lens or to any weighted combinations of them.

The edge detection metalens phase profile is achieved by exploiting the geometric phase mechanism, of which the modulated phase is twice the rotation angle of the nanobars. [39,40] In the proposed design, the optimized nanobar geometry has a length (L) of 180 nm, a width (W) of 80 nm, and a unit (U) cell size of $300 \times 300 \text{ nm}^2$, as depicted in Figure 2c. Figure 2d shows the wavelength-dependent reflectance of copolarized and cross-polarized light, indicating the best edge detection performance around 800 nm. To realize intensity manipulated imaging, a layer of TiN/Al₂O₃ metallic quantum wells with high Kerr nonlinearity is employed as the tunable material, whose complex refractive indexes change from metallic to dielectric as the input power increases. With metallic layer thickness approaching the de Broglie wavelength, the free electrons in the metal film are quantized into discrete energy levels and the intersubband transition frequency can be predicated by the quantum electrostatic model.[41] The giant Kerr-type nonlinearity in metallic quantum well system mainly stems from the intersubband transition and can be aligned at the desired wavelength by tuning the quantum well thickness.^[38] In this work, 2.4 nm TiN quantum wells are chosen for the computational metalens, enabling intersubband transition enhanced giant Kerr nonlinearity with working wavelength also around 800 nm. The Z-Scan experiment for the nonlinear property is described in Supporting information, Section S3. The thickness ratio between TiN and Al₂O₃ (1 nm) is selected to achieve a large tuning range of the phase retardation ϕ . The

simulation result of the designed sample can be found in the Section S4 of Supporting Information (Finite element method simulations).

The fabrication processes of the nonlinear computational metalens are all carried out in a standard cleanroom. The device is fabricated on a sapphire (Al₂O₃) substrate. A 6-pair TiN/ Al₂O₃ quantum well (transmission electron microscopes image shown in Figure 1b), is sandwiched between a gold reflector (20 nm) at the bottom and an Al₂O₃ spacer layer (90 nm) on the top. On top of the spacer layer, an array of gold nanobars is fabricated with electron beam lithography followed by film deposition (30 nm) and a lift-off process. More details related to sample fabrication can be found in the Section S5 (Supporting Information). The total pattern size of the metalens is around $500\times500~\mu\text{m}^2$, as shown in Figure 2e. Figure 2f is the scanning electron microscope (SEM) image of the final fabricated metalens.

To verify the edge detection capability of the designed metalens, the transfer function of the metalens is measured and compared with theoretical calculation. Figure 3a,b is the calculated object intensity distribution and the resulting edge images which clearly show the edges of the circular object along two diagonal directions. The calculated transfer function and its line profile are shown in Figure 3c,d. The experimental results are organized in Figure 3e–h, showing good agreement with the simulated one. Details related to transfer function measurement can be found in the Section S6 of Supporting Information. The adjustable edge detection resolution of the metalens is demonstrated in Figure 3I,k by characterizing two designs with different phase profiles. A United States Air Force target

www.afm-iournal.de

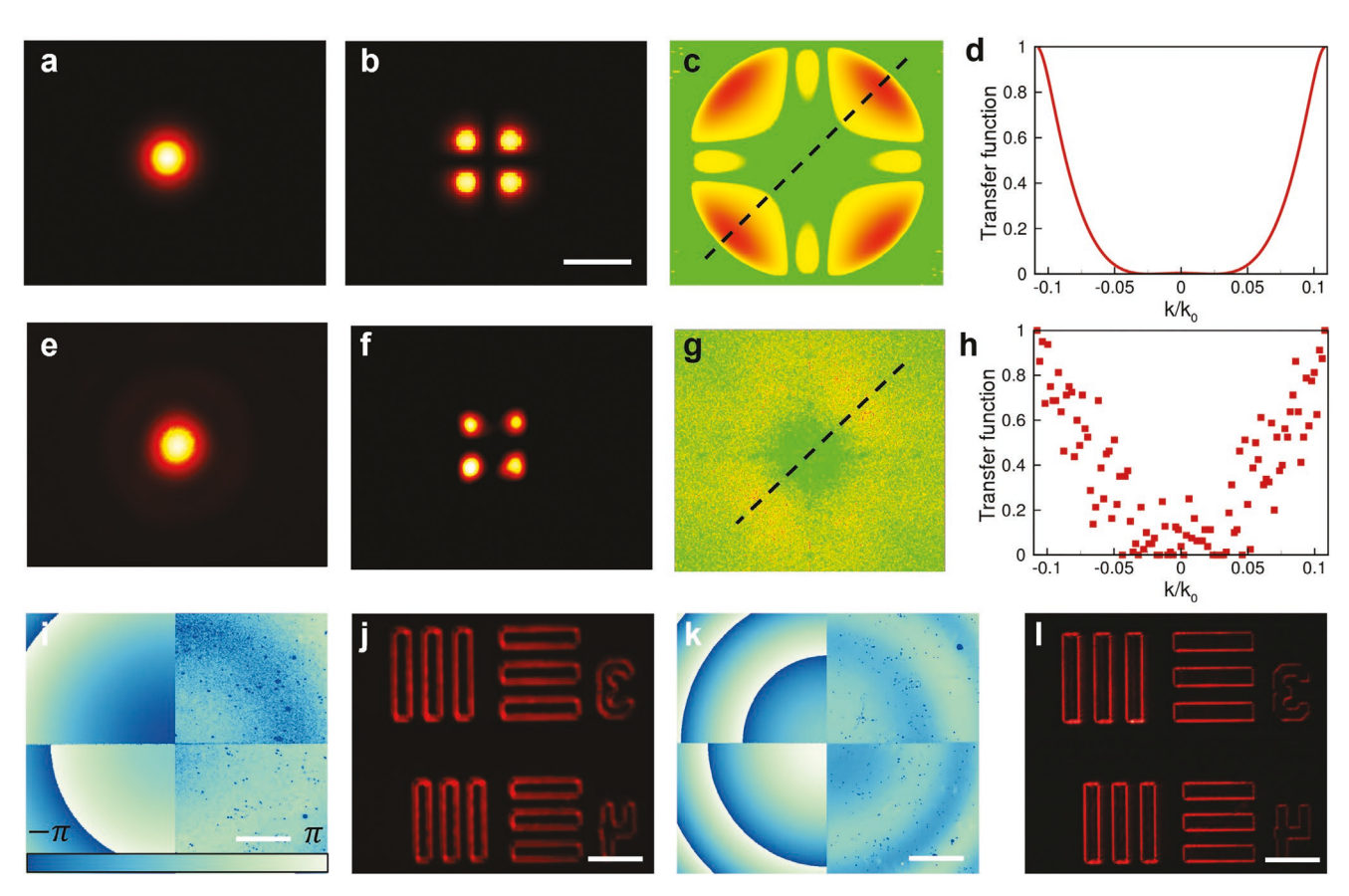


Figure 3. The edge detection performance of the metalens at low intensity at the wavelength of 800 nm. a–d) Theorical results. The incident Gaussian beam a) without and b) with the metalens. The 2D transfer function map c) and the corss-section plot d) along the marked dashed line in c). e–h) Experimental measurements compared with a–d). i–l) Edge detection with different resolutions. i,k) The phase image of the designed metalenses with different parameters. Scale bar, 20 μm. j,l) Edge images by using metalens in i,k), respectively. Scale bar, 300 μm.

is used as the object. Figure 3I,k displays the calculated phase profiles based on Equation (3) juxtaposed with the measured dark-field scattering images of the metalens. The simulated phase distribution is also provided in the Section S7 of Supporting Information. Under linear polarized dark-field illumination, the scattering effeciency of the nanoantennas varies with respect to their geometric orientations, which reveals the local phase distribution of the fabricated metalens. Each quadrant of the metalens contains a laterally-shifted lens phase and is out of phase with the neighboring quadrants to realize the differentation function. The edge detection resolution is determined mainly by the spatial shift of the focal position and the focal length of the metalens in each quadrant. The metalens shown in Figure 3i has a lateral focal shift Δ of 35 μm with a 20 mm focal distance. The metalens shown in Figure 3k is designed with a smaller lateral focal shift Δ of 5 μm with a 10 mm focal distance. The edge resolution 2Δ is close to the diffraction limit resolution of 8.1 µm. Figure 3j,l presents the edge detection images using the two metalens shown in Figure 3I,k correspondingly. The measurement setup is shown in the Section S8 of Supporting Information.

Figure 4 shows the simulated weighting property of the proposed nonlinear computional metalens. As predicated in Equation (2), the output of the metalens at the image plane is the weighted sum of a diffracted electric field with weighting

 $cos(\Phi/2)$ and an edge-detected electric field of the object with weighting $\sin(\Phi/2)$. Therefore, here we compare the coherent transfer funtions (CTF) of the two electric fields with respect to the weighting (Figure 4a) tuned by the intensity dependent phase retardation Φ . As the intensity is increased, the CTF of the imaging system gradually transforms from a high pass filter to an all pass filter so that the resulting image transfroms from edge-detection to free space diffraction, as shown in Figure 4b-p. A complex object shown in Figure 4q,r is used to demonstrate the power dependent imaging ouput. Under low illumination intensity, the edge image of both the amplitude and phase components of the input image is generated. As presented in Figure 4s-w, with increasing intensity, the diffraction component gradually dominates the output image. Eventually, only the free space diffraction of the object is observed.

Figure 5a shows the change of phase retardation between the long- and short-axis polarizations when the input intensity is increased. The experimental intensity dependent material property is provided in Section S9 of Supporting Information. The image differentiator works at its highest efficiency when the phase retardation between the two polarizations is π . As predicted by Equation (3), with increasing light intensity, the phase retardance Φ gradually deviates from π , causing a reduction in the phase contrast of the metalens, as simulated in Figure 5b–e.

www.advancedsciencenews.com www.afm-journal.de

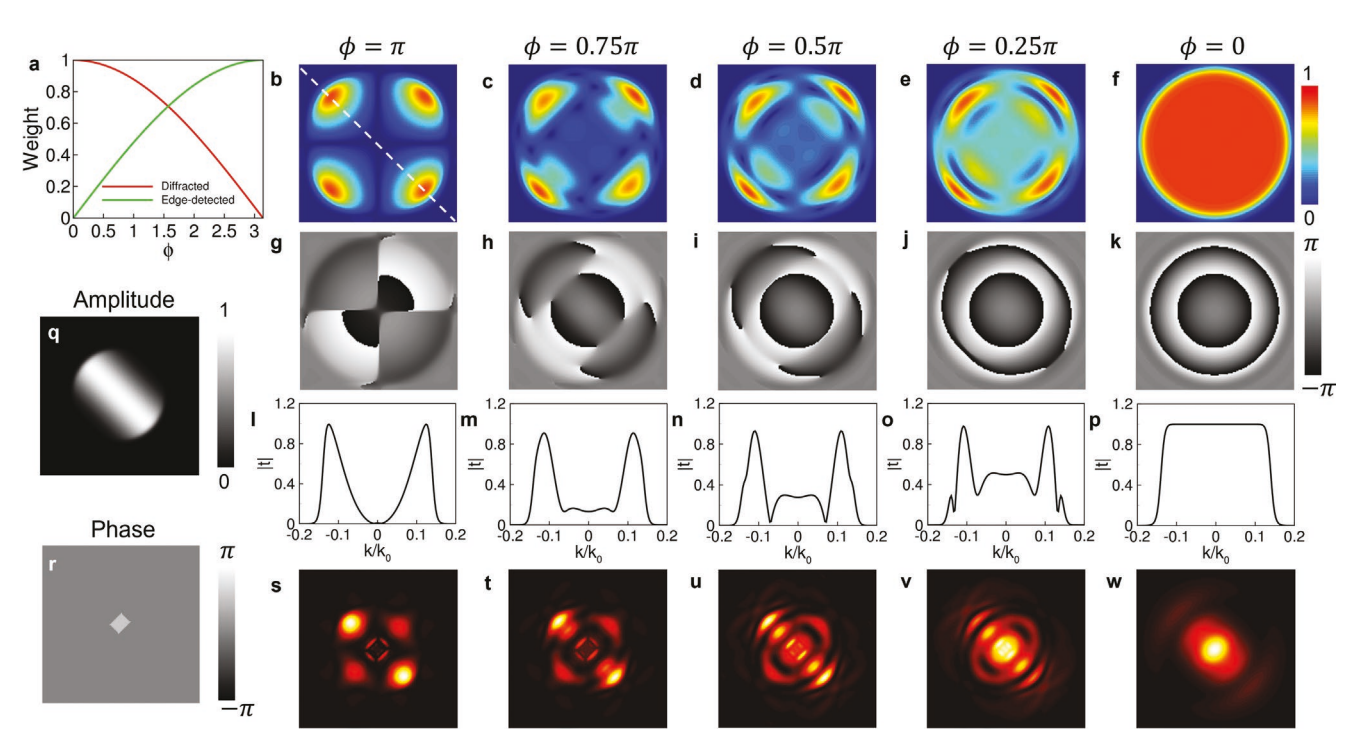


Figure 4. Simulated nonlinear computational metalens with a lateral focal shift Δ of 5 μ m with a 10 mm focal distance performance. a) The weight of diffracted and edge detected components depending on Φ . b–f) The amplitude and g–k) the phase of the CTF dependent on intensity-controlled phase retardation Φ . l–p) Cross section along the dashed line of b–f). q–f) The intensity and phase distribution of an examplary simulated object. s–w) The coresponding far field at the image plane intensity distribution with respect to different phase retardation.

In consequence, the edge detection image gradually transforms into a diffracted full image of the object, as shown in Figure 5g–j.

3. Discussion and Conclusion

The current device can be made more useful in practice by improving several design aspects. First, the metallic quantum wells layer is the biggest source of insertion loss. The total reflectance efficiency of the device is measured around 40%

(60% insertion loss). By replacing metallic quantum wells layer with less lossy nonlinear material, the total efficiency could be improved dramatically. [42] Second, transmission mode metalens based on dielectric nanostructures with high efficiency with our proposed phase design could further compact the imaging system. Finally, a wide range of other mathematical operations can be realized by similar design principle. For example, instead of differentiator demonstrated in this work, tunable optical integrator with nonlinear response to input function can be achieved with different nonlinear metalens design. [43]

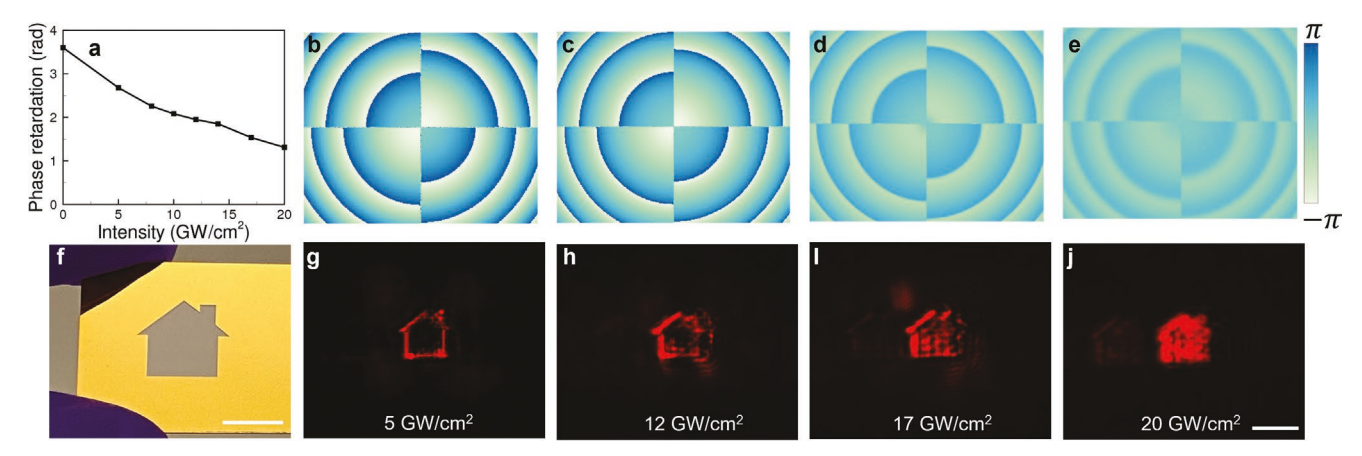


Figure 5. Nonlinear computional metlens performance at the wavelength of 800 nm. a) The intensity-dependent phase retardation Φ . b—e) The phase distribution of the metalens at the different intensity. f) The used object, Scale bar, 1 cm. g—j) The captured image tuned by the incident intensity, scale bar, 200 μ m.



www.advancedsciencenews.com

www.afm-iournal.de

ADVANCED FUNCTIONAL MATERIALS

In this paper, we experimentally demonstrate the first tunable computational metalens based on optical nonlinearity, which performs different computational imaging by changing the CTF of the imaging system based on the illumination intensity. Compared to other optical computation methods such as Fourier optical system which require bulky optical components and do not possess tunability, our design has two major advantages. First, this design performs analog image processing using a single device and reduces the size of the imaging system tremendously. Second, thanks to the highly nonlinear metamaterial, the CTF of the imaging system is actively tuned by light intensity to achieve different computed imaging results. The idea of performing tunable analog optical computation by using optical nonlinearity can be extended to many other optical computations. For example, metalens together with nonlinear metamaterial provides a versatile platform to implement complex nonlinear activation functions, which are highly sought for optical neural networks as they enable more complex mappings between the network's inputs and outputs. Additionally, the nonlinear metalens can fit into many highly integrated systems to replace conventional optics and the necessity for Electric-Optical-Electric conversion in many components, allowing real-time mathematical operations on the analog signals at high speed.

Supporting Information

Supporting Information is available from the Wiley Online Library or from the author.

Acknowledgements

This work was partially supported by the NSF-ECCS-1907423.

Conflict of Interest

The authors declare no conflict of interest.

Author Contributions

Z. L. and J. Zhou proposed the idea. J. Zhou and Q. W. did the theorical and simulation parts. J. Zhou and C. C. built the experiments setup and did the measurement. J. Zhou, J. Zhao and M. L. conducted the metalens characterization. J. Zhou and C. C. designed and fabricated the object mask. J. Zhou analyzed the experiment data. J. Zhou, Q. W., G. C., and F. T. prepared all the figures. All the authors discussed the results and prepared the paper.

Data Availability Statement

The data that support the findings of this study are available in the supplementary material of this article.

Keywords

edge detection, metalens, nonlinear

Received: April 26, 2022 Revised: May 22, 2022 Published online:

- [1] F. L. Pedrotti, L. M. Pedrotti, L. S. Pedrotti, *Introduction to Optics*, Cambridge University Press, Cambridge, England **2017**.
- [2] J. W. Goodman, Introduction to Fourier Optics, Roberts and Company Publishers, Englewood, CO 2005.
- [3] Y. Zhou, H. Zheng, I. I. Kravchenko, J. Valentine, *Nat. Photonics* 2020, 14, 316.
- [4] C. Guo, M. Xiao, M. Minkov, Y. Shi, S. Fan, Optica 2018, 5, 251.
- [5] T. Zhu, Y. Zhou, Y. Lou, H. Ye, M. Qiu, Z. Ruan, S. Fan, Nat. Commun. 2017, 8, 15391.
- [6] D. Xu, S. He, J. Zhou, S. Chen, S. Wen, H. Luo, Opt. Lett. 2020, 45, 6867.
- [7] T. Zhu, C. Guo, J. Huang, H. Wang, M. Orenstein, Z. Ruan, S. Fan, Nat. Commun. 2021, 12, 680.
- [8] D. Xu, S. He, J. Zhou, S. Chen, S. Wen, H. Luo, Appl. Phys. Lett. 2020, 116, 211103.
- [9] T. Zhu, Y. Lou, Y. Zhou, J. Zhang, J. Huang, Y. Li, H. Luo, S. Wen, S. Zhu, Q. Gong, Phys. Rev. Appl. 2019, 11, 034043.
- [10] S. He, J. Zhou, S. Chen, W. Shu, H. Luo, S. Wen, Opt. Lett. 2020, 45, 877
- [11] S. He, J. Zhou, S. Chen, W. Shu, H. Luo, S. Wen, APL Photonics 2020, 5, 036105.
- [12] N. Yu, P. Genevet, M. A. Kats, F. Aieta, J.-P. Tetienne, F. Capasso, Z. Gaburro, *Science* 2011, 334, 333.
- [13] D. Lin, P. Fan, E. Hasman, M. L. Brongersma, Science 2014, 345, 298
- [14] J. Rensberg, S. Zhang, Y. Zhou, A. S. McLeod, C. Schwarz, M. Goldflam, M. Liu, J. Kerbusch, R. Nawrodt, S. Ramanathan, D. N. Basov, F. Capasso, C. Ronning, M. A. Kats, *Nano Lett.* 2016, 16, 1050.
- [15] M. Zhou, J. Liu, M. A. Kats, Z. Yu, ACS Photonics 2017, 4, 1279.
- [16] S. Wang, P. C. Wu, V.-C. Su, Y.-C. Lai, M.-K. Chen, H. Y. Kuo, B. H. Chen, Y. H. Chen, T.-T. Huang, J.-H. Wang, R.-M. Lin, C.-H. Kuan, T. Li, Z. Wang, S. Zhu, D. P. Tsai, *Nat. Nano-technol.* 2018, 13, 227.
- [17] W. T. Chen, A. Y. Zhu, V. Sanjeev, M. Khorasaninejad, Z. Shi, E. Lee, F. Capasso, Nat. Nanotechnol. 2018, 13, 220.
- [18] P. Yu, J. Li, X. Li, G. Schütz, M. Hirscher, S. Zhang, N. Liu, ACS Nano 2019, 13, 7100.
- [19] K.-T. Lee, M. Taghinejad, J. Yan, A. S. Kim, L. Raju, D. K. Brown, W. Cai, ACS Photonics 2019, 6, 2663.
- [20] S. Lan, X. Zhang, M. Taghinejad, S. Rodrigues, K.-T. Lee, Z. Liu, W. Cai, ACS Photonics 2019, 6, 864.
- [21] P. Yu, J. Li, N. Liu, Nano Lett. 2021, 21, 6690.
- [22] L. Jing, X. Lin, Z. Wang, I. Kaminer, H. Hu, E. Li, Y. Liu, M. Chen, B. Zhang, H. Chen, *Laser Photonics Rev.* 2021, 15, 2000426.
- [23] F. Z. Shu, J. N. Wang, R. W. Peng, B. Xiong, R. H. Fan, Y. J. Gao, Y. Liu, D. X. Qi, M. Wang, Laser Photonics Rev. 2021, 15, 2100155.
- [24] W. T. Chen, A. Y. Zhu, J. Sisler, Z. Bharwani, F. Capasso, Nat. Commun. 2019, 10, 355.
- [25] J. Li, G. Wang, Z. Yue, J. Liu, J. Li, C. Zheng, Y. Zhang, Y. Zhang, J. Yao, Opto-Electron. Adv. 2022, 5, 210062.
- [26] J. Zhou, H. Qian, C.-F. Chen, J. Zhao, G. Li, Q. Wu, H. Luo, S. Wen, Z. Liu, Proc. Natl. Acad. Sci. USA 2019, 116, 11137.
- [27] P. Huo, C. Zhang, W. Zhu, M. Liu, S. Zhang, S. Zhang, L. Chen, H. J. Lezec, A. Agrawal, Y. Lu, T. Xu, Nano Lett. 2020, 20, 2791.
- [28] J. Zhou, S. Liu, H. Qian, Y. Li, H. Luo, S. Wen, Z. Zhou, G. Guo, B. Shi, Z. Liu, Sci. Adv. 2020, 6, eabc4385.
- [29] A. Komar, R. A. Aoni, L. Xu, M. Rahmani, A. E. Miroshnichenko, D. N. Neshev, ACS Photonics 2021, 8, 864.
- [30] J. Zhou, H. Qian, J. Zhao, M. Tang, Q. Wu, M. Lei, H. Luo, S. Wen, S. Chen, Z. Liu, *Natl. Sci. Rev.* **2021**, *8*, nwaa176.



www.advancedsciencenews.com www.afm-journal.de

ADVANCED FUNCTIONAL MATERIALS

- [31] Q. He, F. Zhang, M. Pu, X. Ma, X. Li, J. Jin, Y. Guo, X. Luo, Nanophotonics 2021, 10, 741.
- [32] Y. Zhou, W. Wu, R. Chen, W. Chen, R. Chen, Y. Ma, Adv. Opt. Mater. 2020, 8, 1901523.
- [33] M. K. Chen, Y. Yan, X. Liu, Y. Wu, J. Zhang, J. Yuan, Z. Zhang, D. P. Tsai, Nanophotonics 2021.
- [34] H. Kwon, D. Sounas, A. Cordaro, A. Polman, A. Alù, Phys. Rev. Lett. 2018, 121, 173004.
- [35] F. Zangeneh-Nejad, D. L. Sounas, A. Alù, R. Fleury, Nat. Rev. Mater. 2021, 6, 207.
- [36] Y. Zuo, B. Li, Y. Zhao, Y. Jiang, Y.-C. Chen, P. Chen, G.-B. Jo, J. Liu, S. Du, Optica 2019, 6, 1132.
- [37] X. Sui, Q. Wu, J. Liu, Q. Chen, G. Gu, IEEE Access 2020, 8, 70773.
- [38] S. Li, H. Qian, Z. Liu, Adv. Funct. Mater. 2020, 30, 2000829.
- [39] M. V. Berry, Proc. R. Soc. London, Ser. A 1984, 392, 45.
- [40] S. Pancharatnam, Proc. Indian Acad. Sci., Sect. A 1956, 44, 398.
- [41] H. Qian, Y. Xiao, Z. Liu, Nat. Commun. 2016, 7, 13153.
- [42] M. Z. Alam, I. De Leon, R. W. Boyd, Science 2016, 352, 795.
- [43] A. Pors, M. G. Nielsen, S. I. Bozhevolnyi, Nano Lett. 2015, 15, 791.